High Volume Rate, High Resolution 3D Plane Wave Imaging

Ming Yang*, Richard Sampson†, Siyuan Wei*,
Thomas F. Wenisch†, Brian Fowlkes‡, Oliver Kripfgans‡, and Chaitali Chakrabarti*

*School of ECEE, Arizona State University, Tempe, AZ, 85287
†Department of EECS, University of Michigan, Ann Arbor, MI, 48188
‡Department of Radiology, University of Michigan, Ann Arbor, MI 48109

***Abstract*—3D plane-wave imaging systems can support the high volume acquisition rates that are essential for 3D vector flow imaging and sonoelastography but suffer from low resolution and low SNR. Coherent compounding is a technique to improve the image quality of plane-wave systems at the expense of significant increase in beamforming computational complexity. In this paper, we propose a new separable beamforming method for 3D plane-wave imaging with coherent compounding that has computational complexity comparable to that of a non-separable non-compounding baseline system. The new method with 9-fire-angle compounding helps improve average CNR from 1.6 to 2.2 and achieve a SNR increase of 9.0 dB compared to the baseline system. We also propose several enhancements to our beamforming accelerator, Sonic Millip3De, including additional SRAM arrays, configurable interconnect, and embedded DRAM. Overall, our system is capable of generating high resolution images at 1000 volumes per second.**

I. Introduction

3D vector flow imaging and 3D elastography require high volume acquisition rates of over 1000 volumes per second. 3D plane-wave imaging has the potential to achieve such high volume acquisition rates because it utilizes a defocused plane-wave excitation and produces multiple scanlines in each firing. Unfortunately, plane-wave imaging systems suffer from low resolution and low SNR due to lack of transmit focus. A coherent image compounding scheme was proposed in [1] to compensate for the lower quality of plane-wave based 2D imaging systems at the expense of significant increase in computational complexity.

In this paper, we propose a low complexity 3D plane-wave imaging system that applies coherent image compounding to improve lateral resolution and SNR. We offset the increased computation requirement of compounding by applying separable beamforming. In our earlier work, we proposed a separable beamforming algorithm for plane-wave systems based on the delay decomposition that achieves minimum root-mean-square (RMS) phase error, which significantly reduces the computational complexity [2]. In this paper we present a new delay decomposition for separable beamforming that is able to capture the effect of angled plane-wave firing required by coherent image compounding. Use of the new separable beamforming method helps achieve 11× reduction in computation, creating headroom to compound multiple images. The Field II simulations show that the proposed system with 9-firing-angle compounding has better image quality in terms of sidelobe levels, SNR values, and contrast-to-noise ratios (CNR), while having lower computational complexity compared to the baseline (non-separable, non-compounded) plane wave system.

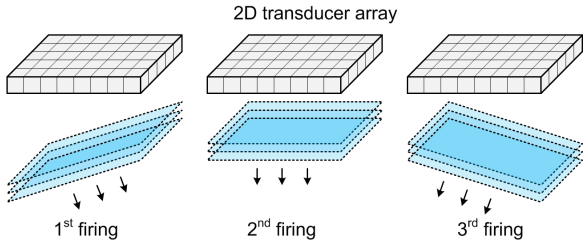

Fig. 1. Firing scheme of 3D plane-wave system with compounding

We also present hardware modifications to the Sonic Millip3De accelerator originally designed for synthetic aperture ultrasound (SAU) systems [3]. These include additional low power embedded DRAM and a configurable interconnect to support on-chip compounding and separable beamforming. These architecture level upgrades allow us to achieve 1000 volumes per second.

II. Separable Beamforming with Coherent Image Compounding

A. Plane-wave 3D Imaging and Coherent Compounding

During transmit of a 3D plane-wave system, all transducers in the selected aperture fire and emulate a plane wave that is parallel to the transducer plane. All the elements in the selected aperture receive the echo signals. Subsets of elements within the selected aperture form a sequence of beamforming apertures, traversing all possible positions within the selected aperture. The size of the beamforming aperture increases dynamically with image depth to maintain consistent resolution across depths. In each position, the beamforming aperture generates a single vertical scanline located at its center. When part of the beamforming aperture is outside the selected aperture, the corresponding apodization coefficients are set to zero. A 3D plane-wave system with coherent image compounding fires the plane wave at multiple firing angles as shown in Fig. 1. The volumes obtained by these firings are coherently combined resulting in improved SNR and lateral resolution.

B. Delay Decomposition for Separable Beamforming with Coherent Compounding

The scanline geometry of a 3D plane-wave system is shown in Fig. 2a. In this system, the scanlines are all parallel to each other and perpendicular to the transducer plane. $(x, y, 0)$ is the coordinate of a transducer element, and $(\hat{x}, \hat{y}, \hat{z})$ is the

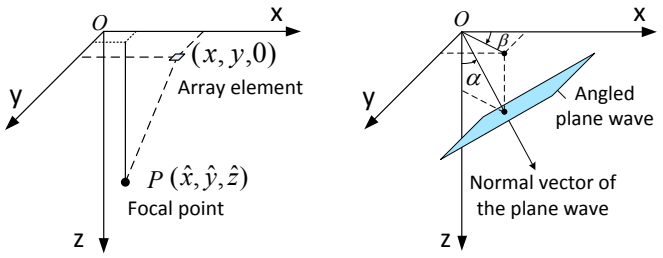

(a) Coordinate system (b) Firing plane angles

Fig. 2. Coordinate system and angle definition of 3D plane-wave system with coherent compounding

coordinate of focal point P. The plane wave firing angles can be defined by (α, β) as shown in Fig. 2b, where α is the angle between the z axis and the normal vector, and β is the angle between the x axis and the projection of the normal vector on the xy plane.

The beamforming delay is given by $\tau = (2|\hat{z}| - d_{tx} - d_{rx})/c$, where c is the speed of sound, d_{tx} is the distance between the wavefront plane and the focal point P at $t = 0$, and d_{rx} is the distance between the focal point P and the receive transducer at $(x, y, 0)$. d_{tx} and d_{rx} are calculated as follows.

$$d_{tx}=(\hat{x} - x_0)\sin\alpha\cos\beta + (\hat{y} - y_0)\sin\alpha\sin\beta + (\hat{z} - z_0)\cos\alpha \quad (1)$$

$$d_{rx}=\sqrt{(x - \hat{x})^2 + (y - \hat{y})^2 + \hat{z}^2} \quad (2)$$

where (x_0, y_0, z_0) is the coordinate of an arbitrary point on the wavefront at $t = 0$. Thus, the beamforming delay τ is a function of five variables, namely $\tau(x, y, \hat{x}, \hat{y}, \hat{z})$. Assuming the receive signal at transducer (x, y) is $S(x, y, t)$, the non-separable beamforming process for a plane wave system is represented by

$$F(\hat{x}, \hat{y}, \hat{z}; t) = \int_{\hat{y}-\frac{D_y}{2}}^{\hat{y}+\frac{D_y}{2}} \int_{\hat{x}-\frac{D_x}{2}}^{\hat{x}+\frac{D_x}{2}} A(x - \hat{x}, y - \hat{y}) \cdot S(x, y, t - \tau(x, y, \hat{x}, \hat{y}, \hat{z}))dxdy \quad (3)$$

where D_x and D_y are the width of the beamforming aperture in x dimension and the height of the beamforming aperture in y dimension, respectively.

Now if the delay term can be decomposed as

$$\tau(x, y, \hat{x}, \hat{y}, \hat{z}) \approx \tau_1(x, y, \hat{x}, \hat{z}) + \tau_2(y, \hat{x}, \hat{y}, \hat{z}) \quad (4)$$

and apodization coefficients can be represented by $A(x-\hat{x}, y-\hat{y}) = A_x(x - \hat{x}) \cdot A_y(y - \hat{y})$, the beamforming process can be decomposed as

$$F^{(1)}(y, \hat{x}, \hat{z}; t) = \int_{\hat{x}-\frac{D_x}{2}}^{\hat{x}+\frac{D_x}{2}} A_x(x - \hat{x})S(x, y, t - \tau_1(x, y, \hat{x}, \hat{z}))dx \quad (5)$$

$$F^{(2)}(\hat{x}, \hat{y}, \hat{z}; t) = \int_{\hat{y}-\frac{D_y}{2}}^{\hat{y}+\frac{D_y}{2}} A_y(y - \hat{y})F^{(1)}(y, \hat{x}, \hat{z}; t - \tau_2(y, \hat{x}, \hat{y}, \hat{z}))dy \quad (6)$$

Fig. 3 demonstrates this process. In the first stage, beamforming is performed along the x dimension. The 1-D beamforming aperture traverses the entire selected aperture. For each combination of $(\hat{x}, y)$, a 1-D beamformer steers the azimuth angle to be normal to the xy plane, and records partially beamformed data in $F^{(1)}(y, \hat{x}, \hat{z}; t)$. In the second-stage, the 1-D beamforming aperture moves along the y dimension. For each combination of $(\hat{x}, \hat{y})$, the beamformer steers the elevation angle to be normal to the xy plane and a scanline is generated.

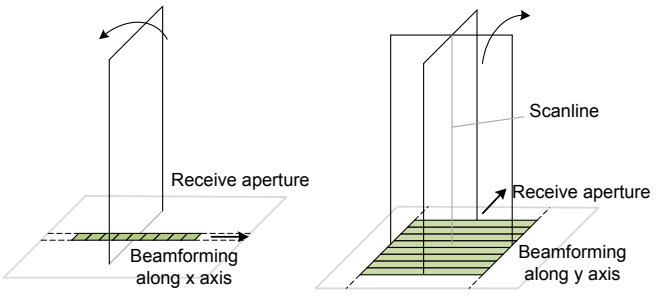

(a) Stage 1: azimuth steering (b) Stage 2: elevation steering

Fig. 3. The principle of plane-wave separable beamforming

For a 3D plane-wave system without coherent image compounding, we had earlier proposed a minimum RMS-based delay decomposition method [2]. The delay τ was a function of three variables, and τ was then decomposed into τ_1 and τ_2, each a function of two variables. Here τ is a function of five variables, to capture the effect of angled plane wave firing, and $\tau_1(x, y, \hat{x}, \hat{z})$ and $\tau_2(y, \hat{x}, \hat{y}, \hat{z})$ are functions of four variables. To reduce the approximation error due to this decomposition, the significant cross terms in the Taylor series expansion of the beamforming delay function should be kept. The functions τ, τ_1 and τ_2 all contain $\hat{z}$. τ_1 contains x and $\hat{x}$, because after first-stage beamforming along x, the beamformer is able to focus in the vertical azimuth angle at position $\hat{x}$ (recall Fig. 3a). Adding y to the list helps to keep the cross terms due to the square root operation. Similarly, τ_2 contains y and $\hat{y}$, and adding $\hat{x}$ to variable list of τ_2 helps keep cross terms such as $\hat{x}y$ or $\hat{x}\hat{y}$.

To get the optimal solution for τ_1 and τ_2, we minimize the RMSE, which is equivalent to minimizing the error function below.

$$E(y, \hat{x}, \hat{z}) = \int_{y-\frac{D_y}{2}}^{y+\frac{D_y}{2}} \int_{\hat{x}-\frac{D_x}{2}}^{\hat{x}+\frac{D_x}{2}} [\tau(x, y, \hat{x}, \hat{y}, \hat{z}) - (\tau_1(x, y, \hat{x}, \hat{z}) + \tau_2(y, \hat{x}, \hat{y}, \hat{z}))]^2 dxd\hat{y} \quad (7)$$

The discrete version of a solution to this problem is given by:

$$\tau_1(n_x, n_y, m_{\hat{x}}, m_{\hat{z}})=\frac{1}{N_y}\sum_{m_{\hat{y}}=n_y-\frac{N_y}{2}}^{n_y+\frac{N_y}{2}-1} \tau(n_x, n_y, m_{\hat{x}}, m_{\hat{y}}, m_{\hat{z}}) - \rho(n_y, m_{\hat{x}}, m_{\hat{z}}) \quad (8)$$

$$\tau_2(n_y, m_{\hat{x}}, m_{\hat{y}}, m_{\hat{z}})=\frac{1}{N_x}\sum_{n_x=m_{\hat{x}}-\frac{N_x}{2}}^{m_{\hat{x}}+\frac{N_x}{2}-1} \tau(n_x, n_y, m_{\hat{x}}, m_{\hat{y}}, m_{\hat{z}}) - \rho(n_y, m_{\hat{x}}, m_{\hat{z}}) \quad (9)$$

$$\rho(n_y, m_{\hat{x}}, m_{\hat{z}}) =$$

$$\frac{1}{2N_xN_y} \sum_{m_{\hat{y}}=n_y-\frac{N_y}{2}}^{n_y+\frac{N_y}{2}-1} \sum_{n_x=m_{\hat{x}}-\frac{N_x}{2}}^{m_{\hat{x}}+\frac{N_x}{2}-1} \tau(n_x, n_y, m_{\hat{x}}, m_{\hat{y}}, m_{\hat{z}}) \quad (10)$$

where n_x and n_y are transducer column index and row index, respectively; $m_{\hat{x}}$, $m_{\hat{y}}$ and $m_{\hat{z}}$ are scanline column index, scanline row index and focal point index, respectively; N_x and N_y are the number of columns and the number of rows of the transducer array, respectively; $M_{\hat{x}}$ and $M_{\hat{y}}$ are the number of scanlines in x dimension and y dimension, respectively; $M_{\hat{z}}$ is the number of focal point per scanline.

The computation complexity of non-separable beamforming in terms of delay-sum operations per volume is $N_xN_yM_{\hat{x}}M_{\hat{y}}M_{\hat{z}}$. In comparison, separable beamforming requires $N_xN_yM_{\hat{x}}M_{\hat{z}} + N_yM_{\hat{x}}M_{\hat{y}}M_{\hat{z}}$ delay-sum operations per volume, hence the complexity reduction with respect to non-separable beamforming is $N_xM_{\hat{y}}/(N_x + M_{\hat{y}})$. For example, if the beamforming aperture size is 20×20, and the 3D volume has 32×32 scanlines, then separable beamforming results in 12× reduction. As depth increases, the beamforming aperture size increases for a fixed f-number, resulting in a different complexity reduction. Overall, separable beamforming in a plane wave system results in 10–20× reduction in computational complexity.

A direct look-up table implementation of delay calculation in separable beamforming requires storage of 1.4×10^8 delay values for each firing angle. In [3] we proposed an iterative delay calculation method that allows us to calculate the delay values with only three add operations per focal point at the cost of storing some precalculated coefficients. Using a similar technique, the proposed method requires storage of 8.5×10^5 coefficients for each firing angle. Assuming each coefficient has 12 bits on average, this is about 1.2MB storage for each firing angle, and for a system with 9 firing angles, this is about 10.8MB of storage. The storage requirement can be reduced by about 2× if the firing angles are chosen to be symmetric.

C. Modified Sonic Millip3De Hardware Accelerator

In [2]–[4], we proposed Sonic Millip3De, a low-power hardware accelerator capable of producing high-resolution, 3D ultrasound images within a full system power of 15W at the 45nm technology node and projected to achieve the 5W power budge at the 16nm technology node. This high performance and low-power design will enable handheld 3D devices to produce 3D images with a quality comparable to existing 2D imaging devices today while remaining within a power limit safe for contact with human skin. In our previous work on SAU systems [2], we showed how our design can achieve up to 32 volumes per second, capable of supporting real-time 3D ultrasound applications.

The original Sonic Millip3De hardware consists of three 3D-stacked die layers connected vertically using through-silicon vias (TSVs). The first layer comprises of a 2D array of CMUTs and analog components. This layer is connected to a second layer of ADCs and temporary SRAM storage. The third layer consists of a configurable mesh network of 1,024 accelerator units. Each of these accelerator units produce 16 beamformed scanlines for a single transducer using our iterative delay technique [3]. Combining our efficient delay algorithm with the 3D stacked design allows us to achieve massive parallelism, high bandwidth, and low power in a single chip.

In this work, we have expanded our separable beamforming method to handle plane wave systems [2] that produce a much higher volume acquisition rate (greater than 1,000 volumes per second). This increase is due to the simplicity of the separable planar imaging technique as well as a reduction from 96 to 9 firings for a single volume without modifying the underlying algorithm. In our previous system design, sub-volume data from each firing was temporarily stored in off-chip DRAM before being combined to produce the final volume; however, due to the extremely high rate that these sub-volumes are produced for our planar technique (over 9,000 sub-volumes per second), bandwidth to off-chip DRAM is insufficient for temporary storage. To remove this bottleneck, we have modified our design to include an additional 4th die layer of embedded DRAM (eDRAM) to handle the temporary storage of the 21MB sub-volumes locally. Previous work [5] has demonstrated eDRAM as an efficient, high-bandwidth alternative to traditional DRAM in 3D-stacked designs. Additionally eDRAM is more dense and consumes less power than SRAM storage, minimizing the additional power of our modified design. Furthermore, we can avoid the refresh power conventionally required for DRAM since sub-volumes are overwritten so rapidly that there is no need to refresh them.

III. Simulation Results

We evaluate image quality in MATLAB using Field II [6], [7]. The system parameters are listed in Table I. The baseline system employs non-separable beamforming method. The nine plane wave angles are $(\alpha, \beta) \in \{(0°, 0°), (3°, 0°), (6°, 0°), (3°, 90°), (6°, 90°), (3°, 180°), (6°, 180°), (3°, 270°), (6°, 270°)\}$.

TABLE I. System parameters of the 3D plane wave system

Property	Value
Pitch, μm	385
Receive aperture size, transducers	32×32
f-number	2.0
Number of scanlines	32×32
Max depth, cm	5
Center frequency, MHz	4
6 dB transducer bandwidth, MHz	2
A/D sampling rate, MHz	40

In the first simulation case, three point targets are set at depths of 13mm, 23mm, and 33mm. Compared to the baseline system, the non-separable beamforming with compounding provides 9.2 dB SNR improvement, while the separable beamforming with compounding provides 9.0 dB SNR improvement. The xy plane projections of the point spread function at depth of 23mm are shown in Fig. 4. We see that the separable beamforming with coherent compounding method helps to reduce the mainlobe width and the artifacts near the boundary.

Next, three 6mm anechoic cysts located in phantom scatterers at depths of 12mm, 23mm and 33mm are simulated. The CNR values provided by the non-separable beamforming without compounding are 1.8, 1.9 and 1.2, respectively; the

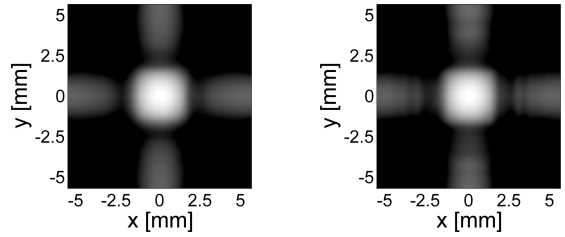

(a) Non-separable beamforming, non-compounding

(b) Separable beamforming, non-compounding

(c) Non-separable beamforming, 9-fire-angle compounding

(d) Separable beamforming, 9-fire-angle compounding

Fig. 4. Point spread functions of non-separable and separable beamforming systems with and without coherent image compounding, displayed in 40 dB dynamic range.

separable beamforming with compounding improves the CNR values to 2.5, 2.4 and 1.7, respectively. The xz slices of the 3D volume are shown in Fig. 5. The image quality of the plane-wave 3D imaging system is significantly improved by the combination of separable beamforming with coherent compounding method.

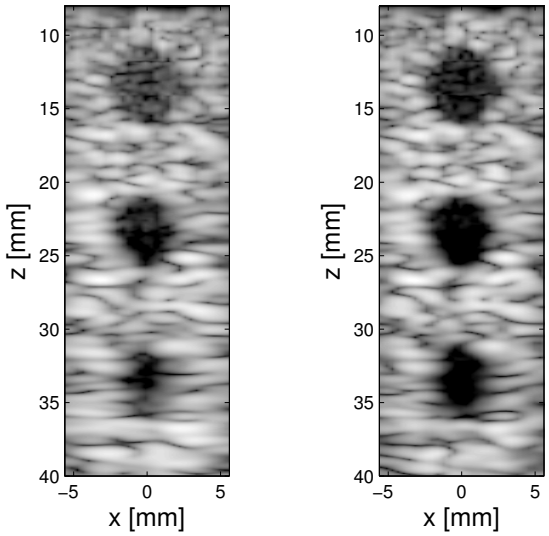

(a) Non-separable beamforming, non-compounding

(b) Separable beamforming, 9-fire-angle compounding

Fig. 5. 2D slices of 3D cyst phantom simulation images

Next we evaluate the computational complexity of our method. The complexity reduction due to separable beamforming is $N_x M_{\hat{y}}/(N_x+M_{\hat{y}})$. Since the beamforming aperture size depends on f-number and depth, the computational complexity is also a function of f-number and depth. Based on the configuration in Table I, for f-number = 2.0 at 10mm depth, $N_x = 13$, and the separable beamforming method reduces computational complexity by about 9×. At 25mm depth, $N_x = 32$, and the complexity reduction is increased to 16×. The overall delay-sum operations per volume required by the non-separable system is about 9.9×10^8, while the delay-sum operations required by separable beamforming is 9.1×10^7, equivalent to 11× reduction per volume.

IV. Conclusion

In this paper, we propose a separable beamforming method in conjunction with coherent image compounding for 3D ultrasound plane-wave imaging systems. Coherent image compounding helps improve resolution and SNR of plane-wave systems, while separable beamforming reduces the beamforming computational complexity for each volume by about 11×. Simulation results show that the proposed method with 9-fire-angle compounding helps improve average CNR from 1.6 to 2.2 and SNR by 9.0 dB with comparable computational complexity compared to the non-separable non-compounding baseline system. We also present the modifications to our beamforming accelerator, Sonic Millip3De, and achieve volume acquisition rates over 1000 volumes per second for the proposed system configuration.

Acknowledgments

This work was supported in part by NSF CCF-1406739, CCF-1406810, CCF-0815457, and CSR-0910699.

References

[1] G. Montaldo, M. Tanter, J. Bercoff, N. Benech, and M. Fink, "Coherent plane-wave compounding for very high frame rate ultrasonography and transient elastography," *IEEE Transactions on Ultrasonics, Ferroelectrics and Frequency Control*, vol. 56, no. 3, pp. 489–506, March 2009.

[2] M. Yang, R. Sampson, S. Wei, T. F. Wenisch, and C. Chakrabarti, "High frame rate 3-D ultrasound imaging using separable beamforming," *to appear in Journal of Signal Processing Systems*, 2014.

[3] R. Sampson, M. Yang, S. Wei, C. Chakrabarti, and T. F. Wenisch, "Sonic Millip3De: Massively parallel 3D stacked accelerator for 3D ultrasound," in *19th IEEE International Symposium on High Performance Computer Architecture*, Feb. 2013, pp. 318–329.

[4] ——, "Sonic Millip3De with dynamic receive focusing and apodization optimization," in *Proceedings of IEEE International Ultrasonics Symposium*, July 2013, pp. 557–560.

[5] D. Fick, R. Dreslinski, B. Giridhar, G. Kim, S. Seo, M. Fojtik, S. Satpathy, Y. Lee, D. Kim, N. Liu, M. Wieckowski, G. Chen, T. Mudge, D. Sylvester, and D. Blaauw, "Centip3De: A 3930DMIPS/W configurable near-threshold 3d stacked system with 64 ARM Cortex-M3 cores," in *Solid-State Circuits Conference Digest of Technical Papers (ISSCC), 2012 IEEE International*, Feb 2012, pp. 190–192.

[6] J. A. Jensen, "FIELD: A program for simulating ultrasound systems," *10th Nordicbaltic Conference on Biomedical Imaging, Vol. 4, Supplement 1, Part 1:351–353*, pp. 351–353, 1996.

[7] J. A. Jensen and N. B. Svendsen, "Calculation of pressure fields from arbitrarily shaped, apodized, and excited ultrasound transducers," *IEEE Transactions on Ultrasonics Ferroelectrics and Frequency Control*, vol. 39, no. 2, pp. 262 –267, Mar. 1992.